Combustion and Flame 213 (2020) 426–440

Contents lists available at ScienceDirect

Combustion and Flame

journal homepage: www.elsevier.com/locate/combustflame

# On the minimum oxygen requirements for oxy-combustion of single particles of torrefied biomass

Aidin Panahi, Neil Toole, Xinyu Wang, Yiannis A. Levendis*

*Mechanical and Industrial Engineering Department, Northeastern University, Boston, MA, USA*

ARTICLE INFO

*Article history:*
Received 11 July 2019
Revised 3 December 2019
Accepted 4 December 2019

*Keywords:*
Biomass
Single particle
Combustion
Oxy-fuel
Torrefied

ABSTRACT

A fundamental investigation was conducted on the combustion characteristics of pulverized torrefied biomass particles both in air and in simulated oxy-combustion gases, containing oxygen and carbon dioxide. Power generation by oxy-combustion of renewable biomass, coupled with carbon-dioxide capture and utilization or sequestration, can contribute to a reduction of the atmospheric concentration of carbon dioxide. This is because renewable biomass absorbs carbon dioxide during its growth, but this method will potentially release almost none to the atmosphere. The goal of this research is to determine the minimum oxygen mole fraction in the furnace input gases, which still induces single particle combustion characteristics that are similar to those encountered in air. Torrefied biomass types were herbaceous, waste crop, and woody. Entire luminous combustion profiles of single particles, burning in a drop-tube furnace, were recorded pyrometrically and cinematographically from ignition to extinction. Combustion took place in two phases: volatiles evolved and burned in spherical envelope flames and, upon extinction of these flames, the residual chars ignited and burned. Replacing the air background gas with 21%$O_2$/79%$CO_2$ prolonged the ignition delay and the burnout time of biomass particles and reduced their temperature. To the contrary, further increasing the oxygen mole fraction in $CO_2$ to 30% caused opposite trends. For each biomass type, the oxygen fraction in $CO_2$ that would produce combustion temperature and time parameters most similar to those of air combustion was projected to be between those two oxygen concentrations (21–30%), and this was verified experimentally. An empirical correlation was formulated to make initial estimates of oxy-combustion concentrations needed for each fuel based on their physical and chemical properties. Reduction of the amount of oxygen in oxy-combustion is important to curtail the energy penalty inflicted by the operation of the air separation unit.



## 1. Introduction

Energy harvesting from combustion of coal currently accounts for roughly 30% of the total electricity generation in the United States [1]. In contrast, energy harvesting from biomass combustion accounts for only ~1.7% of the US total electricity generation [1,2]. Combustion of coal generates and emits large amounts of the greenhouse gas carbon dioxide to the atmosphere [3–5]. Combustion of biomass also emits similar amounts of carbon dioxide, however renewable biomass also absorbs a comparable amount of atmospheric carbon dioxide to grow. Hence, combustion of renewable biomass in utility furnaces can curtail the net emission of carbon dioxide [6,7].

Torrefied biomass was selected for this study as it has some distinct advantages over raw biomass; it has higher energy density, lower hydrophilicity, lower biodegradability, and better grindability [8–10]. Torrefaction is a slow thermal treatment of biomass at moderate temperatures (typically 250–350 °C), during which the fibrous nature of biomass breaks down, its contents of oxygen, chlorine and sulfur are reduced, and its energy density increases [8,11–18]. This process generates a better fuel for storage, transportation, pulverization, fluidization and combustion in a suspension boiler [12,19–23].

In a conventional setting, coal, biomass and their blends are fired within an air-filled furnace, however it is of technological interest to utilize oxy-combustion during this process, if combustion effluents are meant to be utilized or sequestered underground. Oxy-combustion refers to the process of burning the fuels in a mixture of oxygen and dried recycled flue gas (95% $CO_2$) as opposed to ambient air [24–28]. Oxy-combustion is enticing as it requires little modification to traditional boilers, making integrating the method feasible and undemanding [24,29].

Oxy-combustion studies of interest include that of Riaza et al. [29], who burned both raw and torrefied biomass single particle samples in air and $O_2$/$CO_2$ environments, used to simulate

* Corresponding author.
*E-mail addresses:* y.levendis@neu.edu, yal@coe.neu.edu (Y.A. Levendis).

https://doi.org/10.1016/j.combustflame.2019.12.012
0010-2180/

oxy-combustion in order to contrast their combustion behavior. Another study, conducted by Shan et al. [30], analyzed the ignition behavior of single biomass particles, specifically raw pine and raw rice husk. Riaza et al. [31] burned single particles of biomass and measured their burnout times during oxy-combustion at oxygen mole fractions of 21, 30, 35, and 50%.

Studies on the oxy-combustion behaviors of torrefied biomass samples are scarce in the literature. This was a reason that torrefied biomass samples were used within the scope of this research. The study investigated combustion characteristics and parameters of torrefied biomass in both air and simulated oxy-combustion environments. This was accomplished by first making direct measurements of single particle temperatures and burnout times at varying combustion phases of six different torrefied biomass types both in air and in environments containing 21% or 30% oxygen mole fractions in carbon dioxide. Then, based on the recorded combustion temperatures and burnout times, a recommendation for the estimated oxygen concentrations present in oxy combustion that yield parameter values most comparable to standard air combustion for six types of torrefied biomass fuels is given for each biomass. Finally, additional experiments were conducted to verify the recommended values. Finding these oxygen concentration thresholds is important for minimizing the cost of the air separation process. Failing to meet this threshold would lower the overall fuel combustion efficiency and would cause higher amounts of unburned carbon in the fly-ash, whereas surpassing this threshold would cause excess oxygen to be inputted into the environment, driving up operating costs.

It is the underlying hypothesis of this study that these required oxygen mole fractions are directly proportional to chemical and physical properties of the specific fuel. It is also a goal of this work to analyze the yielded concentrations and decipher a correlation between them and several properties at hand. A relationship is sought out to allow the minimum oxygen concentration for oxy-combustion to be predicted for a given biomass fuel, based on the chemical and physical properties that are currently known for each sample within this study. Failure to formulate such a relationship, would signify that the parameters controlling the desirable oxygen levels are either unknown or interrelate too heavily to depict a correlation. Finally, it should be mentioned that in suspension-burning industrial boilers not all of the particles burn at the same rate, as their combustion histories are not similar. Trying to account for this fact, would certainly complicate any analysis. Moreover, the depletion of the oxygen concentration as combustion proceeds can further complicate the interpretation of data [32]. Hence, to minimize such complexities and fundamentally compare the effects of conventional and simulated oxy-combustion atmospheres on the ignition, devolatilization and combustion of pulverized biomass fuels, observations were made on single particles experiencing a constant oxygen partial pressure in the bulk gas.

## 2. Materials and methods

### 2.1. Preparation of samples

In total, six different torrefied biomass variations were utilized in this study to obtain a broad sample of combustion behaviors. Of these samples, three were of the herbaceous type. These include corn straw, miscanthus, and sugarcane bagasse, which were obtained from the Harbin Institute of Technology in China, from Bochum University in Germany, and from a bio-ethanol production plant in Brazil, respectively. Two of the samples, Distiller's Dried Grains with Soluble (DDGS) and rice husk, were of the crop-derived type. The corn-based DDGS was harvested in the USA and was provided by a North American ethanol-producing company. The rice husk was harvested in the Harbin province of China and it was provided by the Harbin Institute of Technology. The last biomass sample present in this study was beechwood, which is categorized as a woody type biomass. The beechwood sample was harvested from trees grown in the Netherlands and it was provided by Bochum University. Torrefaction of all samples was carried out in a laboratory-scale muffle furnace in nitrogen. The furnace was pre-heated to 275 °C (548 K) and thein it was charged with 10–15 mm-size particles of biomass in a wide porcelain boat to ensure sufficient space between particles. Each sample was heat treated at constant conditions for 30 min. Before combustion, all torrefied biomass fuels were air-dried, chopped in a household blender, and

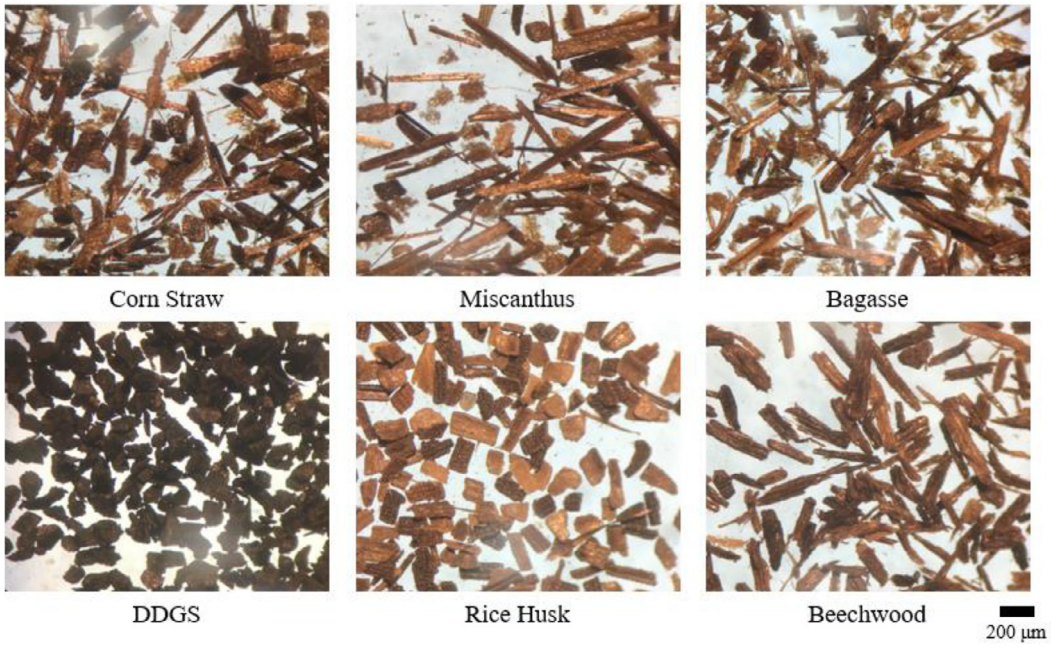


**Fig. 1.** Optical Microscope photographs of the six torrefied biomass fuels utilized within this research.

**Table 1**
Chemical compositions and energy contents of six types of torrefied biomass.

| Rank / Fuel Source | Biomass torrefied in $N_2$ at 275 °C (548 K) for 30 min | | | | | |
|---|---|---|---|---|---|---|
| | Herbaceous | | | Crop-Derived | | Woody |
| | Corn Straw | Miscanthus | Sugarcane bagasse | Corn DDGS | Rice Husk | Beechwood |
| ***Proximate Analysis (dry basis)*** | | | | | | |
| Volatile matter (%) | *67.55* | *75.00* | *73.74* | *71.46* | *55.62* | *72.20* |
| Fixed Carbon (%) | *24.56* | *22.30* | *23.49* | *21.09* | *21.58* | *27.30* |
| Ash (%) | *7.89* | *2.70* | *2.71* | *7.45* | *22.80* | *0.50* |
| ***Ultimate Analysis (dry basis)*** | | | | | | |
| Carbon (%) | *52.77* | *52.80* | *55.82* | *58.22* | *44.16* | *55.40* |
| Hydrogen (%) | *5.32* | *5.70* | *5.45* | *6.32* | *4.41* | *5.30* |
| Oxygen (%) (by difference) | *32.46* | *38.6* | *34.94* | *22.98* | *26.73* | *38.88* |
| Nitrogen (%) | *1.50* | *0.18* | *1.00* | *4.00* | *1.22* | *0.18* |
| Sulfur (%) | *0.07* | *0.46* | *0.03* | *1.01* | *0.03* | *0.31* |
| Calcium (%) | *0.56* | *0.55* | *0.44* | *0.15* | *0.35* | *0.19* |
| Sodium (%) | *0.02* | *0.04* | *0.03* | *0.80* | *0.02* | *0.01* |
| Potassium (%) | *1.19* | *0.97* | *0.06* | *1.50* | *0.73* | *0.19* |
| Magnesium (%) | *0.29* | *0.14* | *0.06* | *0.32* | *0.08* | *0.07* |
| Chlorine (%) | *0.18* | *0.03* | *0.01* | *0.12* | *0.04* | *0.02* |
| Heating Value (MJ/kg) | ***19.4*** | ***20.1*** | ***20.3*** | ***23.7*** | ***16.1*** | ***20.9*** |

size classified by sieving to obtain size cuts of (212–300 μm). This size was selected to minimize the grinding costs, based on the findings of a previous study in this laboratory [33,34]. Optical microscopy photographs of these torrefied fuels can be seen in Fig. 1.

The Proximate and Ultimate analysis of the biomass samples on a dry basis are given in Table 1. Those analyses, as well as the determination of the heating values of the torrefied biomass fuels, were performed at the Harbin Institute of Technology, according to GB/T 212-2008, GB/T 30733-2014, GB/T 30733-2014 and to GB/T 213-2008 Chinese standards, see Ref. [18].

### 2.2. Experimental combustion apparatus

The combustion behaviors of single particles of torrefied biomass samples of this study were monitored in an electrically-heated, laminar drop tube furnace (DTF) manufactured by *ATS*. That furnace is fitted with a water-cooled stainless-steel injector and with a transparent quartz tube with an inner diameter of 7 cm. The length of radiation zone is 25 cm, heated by eight hanging molybdenum heating elements. A schematic of the combustion setup is shown in Fig. 2. Wall temperature, $T_{wall}$, was set at 1400 K due to limitations posed by the use of the transparent quartz tube. At higher temperatures the quartz can turn opaque. This yielded an axial gas temperature within the furnace to be roughly $T_{gas}$ = 1350 K [35]. Fuel particles were entrained in a metered stream of air and gas mixtures ($O_2/CO_2$) of a couple of different oxygen partial pressures. $O_2$ and $CO_2$ gases were supplied by wall-mounted cylinders; their blending proportions were controlled with *Matheson* rotameters, in conjunction with appropriate charts supplied by the manufacturer, and were verified by real-time gas analysis. The flowrate of different gas mixtures ($O_2/CO_2$) was 0.25 L/min through a flow straightener and 0.25 L/min through the furnace injector. Single particles of each biomass fuel were introduced to the system through the injector at the top of the furnace by first placing them on the tip of a beveled needle syringe and then gently tapping the syringe to cause single particles to fall off into the radiation zone. Pyrometric observations of those particles were conducted from the top of the furnace injector, details of the pyrometer optics, electronics, calibration, and performance were given by Levendis et al. [36]. *LabView* software was utilized to process the voltage signals generated by the pyrometer.

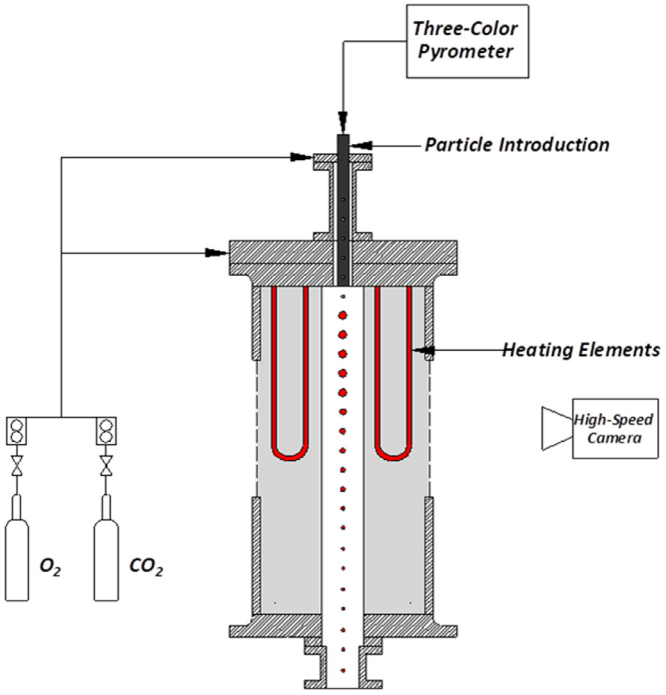


**Fig. 2.** Schematic illustration of the drop tube furnace, particle and sequential photographs of a single particle combustion phase (not to scale).

An *Edgertronic* self-contained digital high-speed broadband video camera was located at one side of the furnace and viewed through slotted side quartz windows to record the particle combustion histories, against a backlight frosted glass positioned at the diametrically-opposite side of the furnace, at speeds of 2000 frames per second. The camera was fitted with an *Olympus-Infinity* model K2 long-distance microscope lens to provide high-resolution images of the combustion events.

## 3. Results and discussion

### 3.1. Cinematographic observations on combustion

Combustion experiments were conducted on single particles of the following six torrefied biomass samples: corn straw,

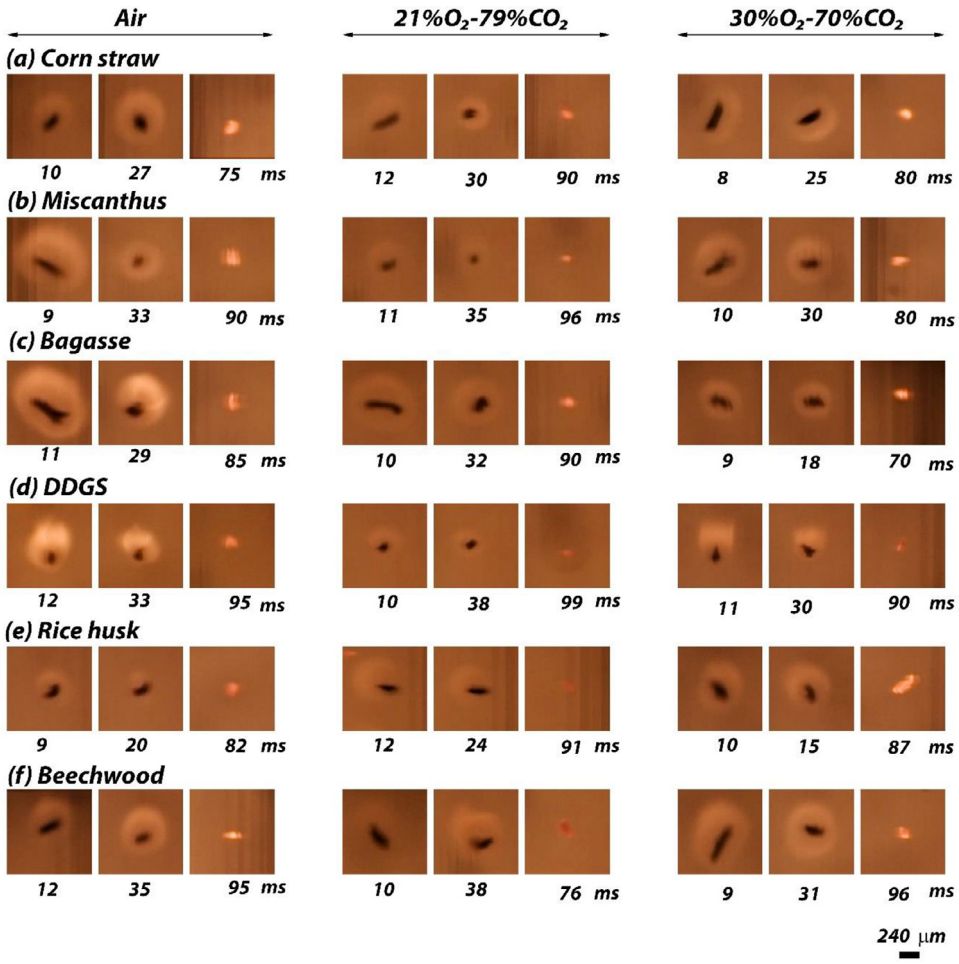


**Fig. 3.** Time-resolved photographic frames from high-speed high-resolution cinematography of single torrefied biomass particles burning in air in a DTF operated at $T_{wall}$ = 1400 K. Numbers under each photographic frame correspond to burn-times in milliseconds, starting from visually-determined ignition. Nominal initial particle sizes were in the range of 212–300 μm.

miscanthus, sugarcane bagasse, DDGS, rice husk and beechwood in air (21%$O_2$-79%$N_2$), as well as in 21%$O_2$-79%$CO_2$ and 30%$O_2$-70%$CO_2$ environments. High-speed, high-resolution cinematographic snapshots of single torrefied biomass particles are shown in Fig. 3. Therein photographic sequences are shown for particles from different biomass types and different background gases, all burning at $T_{wall}$=1400 K, at different instances of their burnout histories. The combustion behaviors of the various types of torrefied biomass particles, which experienced high heating rates ($10^4$ K/s) and high temperatures in the DTF appear to be qualitatively rather similar. This is in line with the findings of Simões et al. [37], who reported that at high heating rates and temperatures the biomass composition becomes less important on some combustion parameters (in their study they examined the ignition mode). This convergence in combustion behavior is perhaps even more pronounced in the case of torrefied biomass, as the torrefaction of biomass generates standardized "coal-like" fuels. This is despite differences in their physical and chemical properties, such as mass, shape, aspect ratios, surface structure and roughness, porosity, volatile content and chemical composition. All torrefied biomass particles in the size range of 212–300 μm, examined herein, appeared to ignite homogeneously and to burn in two phases: volatile matter combustion and char combustion. The particles ignited very close to the injector tip at the top of the DTF, shortly upon entering the radiation zone; measured ignition delays are shown in an ensuing section. Upon ignition, the flames surrounding individual particles grew bigger and increasingly luminous. For all biomass fuels at all gas compositions, the envelope flames exhibited either spherical or ellipsoidal shapes. In cinematographic observations, the volatile flames could be identified easily for these torrefied biomass particles since their volatiles contain tars, which pyrolyzed and formed soot which, in turn, burned with significant luminosity. Upon replacing air with a mixture of 21%$O_2$ / $CO_2$, the particles burned in lower-luminosity spherical envelope flames. The level of luminosity was restored back to that in air when the oxygen mass fraction in carbon dioxide was increased to approach 30%. Upon extinction of the volatile flames, luminous burning of the chars commenced. The appearance of chars is exemplified in Fig. 4(a), where char particles of torrefied Beechwood are shown, collected from flash-pyrolysis of particles in nitrogen inside a similar DTF. It is evident that the occurrence of the phenomena of melting, puffing and spherodization occurred during the pyrolysis of these particles, as also reported earlier [38]. In addition, SEM photographs of ashes from such particles, upon combustion in air inside the DTF are shown in Fig. 4(b).

### 3.2. Combustion phases of the torrefied biomass particles

As torrefied biomass particles went through the combustion process, they experienced two distinct phases known as the volatile phase and the char phase. Throughout their lifetime in the furnace the size and porosity of the individual particles changed as a result of drying, devolatilization, char oxidation and, possibly, char gasification. During the devolatilization phase, short and intense burning of evolving volatile matter took place at high tem-

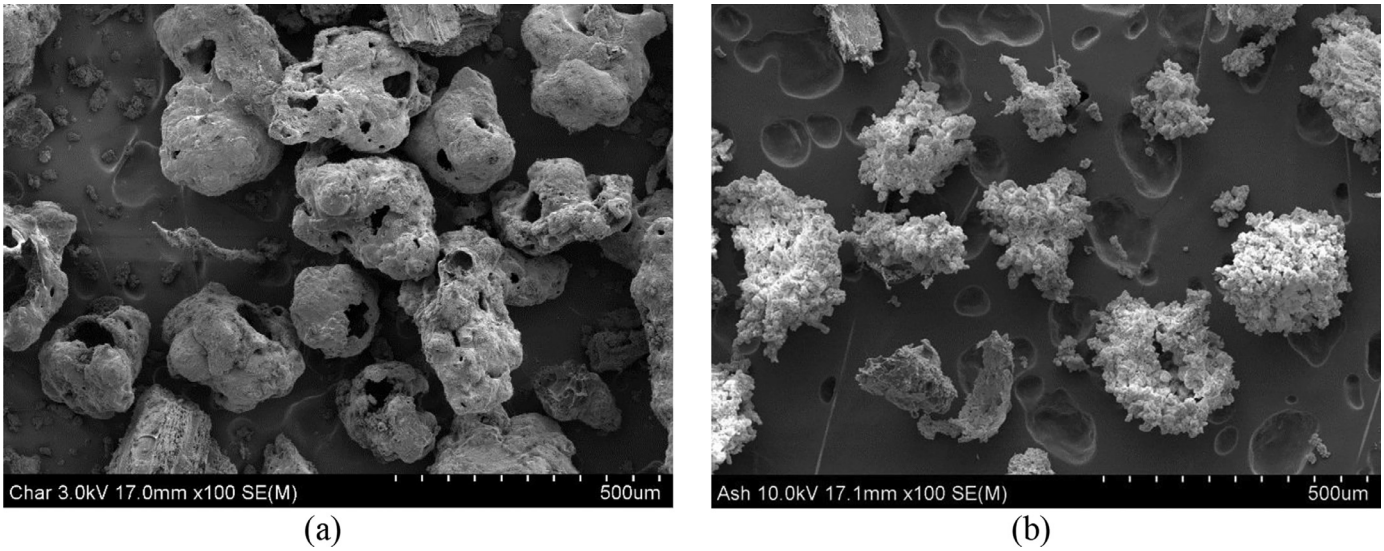


**Fig. 4.** Scanning electron microscope images of particles of torrefied beechwood fuel used in this study (a) char particles upon flash-pyrolysis, (b) ash particles upon combustion in air.

perature and, typically, it did not last as long as the ensuing char combustion phase. This phase can be visually detected in Fig. 3, as the volatile matter burns in luminous envelope flames surrounding the devolatilizing particles. The char phase of the torrefied biomass particles is categorized by a much more prolonged, lower temperature state that lasts for an extended amount of time until the residual carbonaceous particle eventually burns out. Kinetic mechanisms of char oxidation and char gasification are based on char structure and have been developed using experimental information. Oxidation reactions are highly exothermic and drastically increase the char particle temperature. Unlike oxidation reactions, gasification reactions are endothermic and should reduce the char particle temperature. Parenthetically, it has been reported that gasification reactions increase the rate of char oxidation at low oxygen mole fractions and reduce it at oxygen mole fractions above 24% [39,40]. Published kinetic parameters of coal char gasification mechanisms with $H_2O$ and $CO_2$ have been summarized in Ref. [41]. Therein, it was concluded that gasification reactions with $CO_2$ are a thousand times slower than the corresponding oxidation reactions, at furnace conditions and oxygen concentrations similar to those of this study. Hence, gasification reactions were not considered in a simplified char combustion model described in the Appendix of this manuscript. The pyrometric time resolved signals and the deduced temperature-time profiles displayed in Fig. 5 are indicative of the general shape of the profiles for all samples analyzed within this study, displaying an initial, drastic volatile stage followed by a less intense plateau during the char stage. The values present within the legend of said figure relate to three different two-color ratios of the three-wavelength (998, 810 and 640 nm) pyrometer [36]. Particle temperatures both flame and char) were obtained from the pyrometric radiation intensity signals as described in [36,42], using the gray body assumption. These pyrometric temperatures are subject to uncertainties related to both the measurement method and the variabilities in physical and chemical properties in the particle population tested. Either of these uncertainties can be in the order of 100 K, as shown in previous work in this laboratory [33,40].

In this study, several properties relevant to these two stages were of interest. These include the volatile flame temperature seen at the peak of the volatile stage, the char temperature seen at the plateau of the temperature profile during the char oxidation stage, the volatile matter burnout time, the char burnout time, and

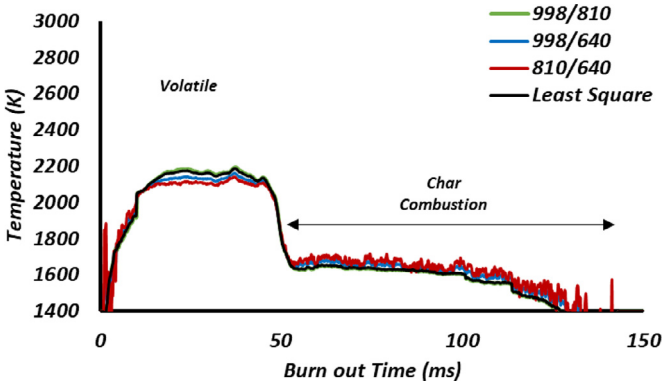


**Fig. 5.** An example of generated temperature-time profiles for a particle of torrefied corn straw burning in air. The particle was in the 212–300 μm size cut. The DTF was operated at $T_{wall}$ = 1400 K.

the total burnout time shown as the time it takes for the particle to go through the entire combustion process. There is significant scatter in the collected data on particle burnout times because of variations in size, shape, mass and, perhaps, composition among the biomass particles in a given size cut. Such variations affect the combustion time durations. To the contrary, there is much less scatter in the temperature data.

### 3.3. Combustion temperatures

Pyrometric temperatures of the volatile envelope flames and chars are presented in Fig. 6. Volatile matter flame temperatures were obtained from pyrometric recordings of the soot radiation originating from such flames. Moreover, the presented values for the volatile flame and char temperatures herein are the peak temperatures measured in single particle pyrometric temperature-time histories, averaged over the 20 single biomass particles that were successfully detected by the pyrometer in each case. Subsequent parameters mentioned within this research were also analyzed with the same number of successful particle readings. In the derivation of such volatile temperatures the gray body assumption was made, based on the findings of Panagiotou et al. [43]. An error analysis on the pyrometric temperatures is presented in Ref. [40].

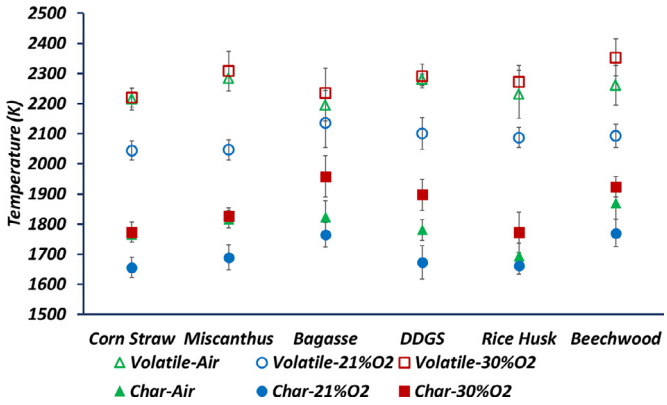


**Fig. 6.** Average measured flame temperatures and char temperatures for all biomass fuels of this study burning with preheated input gases in a DTF, operated at $T_{wall}$ = 1400 K.

Volatile flame temperatures taken at an oxygen concentration of 21% by volume in $CO_2$ were found to be in the range of (2050–2150) K, with some variation occurring depending on the specific type of biomass being analyzed. This range was seen to be noticeably lower than the 30% oxygen concentration flame temperature range, which went from (2200–2300) K. This difference can be attributed to the greater oxygen percentage which allows for more intense combustion to occur. Air combustion yielded volatile flame temperatures in the range of (2150–2300) K, i.e., a little lower than those in the 30%$O_2$/70%$CO_2$ case. Adiabatic flame temperatures were previously calculated for surrogate coal volatile species, using the STANJAN software [44], see Fig. 7 of Ref. [45]. In that study, the combustion of a variety of light hydrocarbons was addressed at a number of different equivalence ratios ($\varphi$ = 0.8, 1.0 and 1.2) to account for the range of fuel/air mixing proportions in the radial direction of the envelope diffusion flames. As increasing the concentration of oxygen (a reactant) increases the burning rate of fuel, by an amount depending on the reaction order, the adiabatic temperature of the flame also increases (e.g., by ~200 K when $O_2$ increases from 21% to 30%). Replacing the background $N_2$ gas with $CO_2$, the adiabatic temperature drops, mostly because of the different physical properties of the gases (e.g., by almost 400 K when $CO_2$ replaces $N_2$ at 21% $O_2$). The measured flame temperatures herein turned out to be lower by 300–500 K than the calculated adiabatic temperatures of stoichiometric mixtures, because of (a) significant heat losses, (b) different composition of pyrolyzates than the surrogate fuels, and (c) departure of local fuel/air compositions from stoichiometry.

Char temperatures behaved similarly to the volatile temperature, with data for air combustion falling in between the 21% and 30% oxygen concentrations in carbon dioxide. For 21% oxygen concentration, the char temperatures ranged from (1650–1750) K, while for 30% oxygen concentration they ranged from (1750–1950) K. Air combustion yielded a char temperature range of (1700–1850) K i.e., lower than those in the 30%$O_2$/70%$CO_2$ case. The range seen for char temperature from air combustion is supported by similar data shown in the past that yielded temperatures within the same span [33]. The specific findings for each individual biomass sample are shown in Fig. 6.

A linear interpolation method was utilized to determine an approximate oxygen percentage that mimics air combustion based on the two concentrations initially analyzed. The specific concentration of oxygen in oxy-combustion that was estimated to produce similar volatile temperature data to that of standard air combustion varies slightly between each type of biomass present within this study in the range of 26–30%. If a similar linear interpolation method is employed to find the desired oxygen percentage in regard to char temperature, such as was done for the volatile flame temperature, it would be found that approximate concentrations in the range of 24–29% are necessary depending on the biomass type.

### 3.4. Combustion burn-out times

The total time that it takes for a single particle to fully complete both phases of the combustion process, known as the burn-out time ($t_{burnout}$), is also a viable parameter to analyze in order to capture the combustion behavior of a biomass fuel. This parameter is a summation of both the volatile matter burnout time and char burnout time. In the 21%$O_2$ oxy-combustion environment, the biomass fuel particles experienced burnout times within the range of (130–250) ms, while particles in the 30%$O_2$ oxy-combustion environment experienced shortened burnout times, in the range of (75–180) ms. These shorter times can be attributed to the more intense combustion behavior that is observed with the higher oxygen percentage. During the biomass particle pyrolysis/devolatilization, it is likely that the flux of volatiles prevented atmospheric oxygen from reaching the forming char, however, oxidation reactions of the carbon with the plentiful fuel-bound oxygen cannot be precluded. When the volatile mater was consumed and the flame was extinguished, char oxidation commenced. Given that the initial diameter of the chars was in the order of 200 μm combustion is likely to have taken place with considerable diffusion limitations, i.e., in Regime III or, possibly, in upper Regime II [46]. In the oxy-combustion cases, the presence of $CO_2$ in the atmosphere can reduce the overall reactivity of both coals. These are the main factors responsible of such a behavior. The higher $CO_2$ heat capacity, in respect of that in $N_2$, reduces the surrounding gas temperature. The lower oxygen binary molecular diffusion in $CO_2$, in respect of that in $N_2$, reduces the $O_2$ flux to the particle and inside the particle, if there is pore penetration, with a resulting decrease of reactivity. Finally, the carbon gasification reactions with $CO_2$ are endothermic and, thus, they lower the char temperature. Combustion conducted in the standard air environment yielded particle burnout times in the range of (120–220 ms). Indeed, such burnout times in 21%$O_2$/79%$N_2$ are shorter than those observed in 21%$O_2$/79%$CO_2$. It should also be mentioned that the DDGS particles experienced the longest combustion times and, also, the highest uncertainty. This is attributed to a clamping tendency exhibited by the particles of this biomass, as observed under microscopy. As a result, some of the observed events may be due to particles stuck together.

When analyzing the specific biomass types, it was estimated that average oxygen concentrations in the range of 24–29% would be necessary to have an oxy-combustion environment mimic air combustion in relation to total burnout time. The specific findings for each individual biomass sample are shown in Fig. 7.

#### 3.4.1. Volatile matter burnout times

The volatile matter burnout time, $t_{v,}$ refers to the amount of time it takes for each particle to complete just the volatile phase of its combustion process. During trials conducted within a 21%$O_2$ oxy-combustion environment, volatile burnout time values were recorded in the range of (30–120) ms, whereas a 30%$O_2$ oxy-combustion environment yielded times in the range of (20–90) ms. Standard air combustion produced volatile times ranging from (30–100) ms, falling within the two thresholds generated by oxy-combustion. A larger degree of variation between biomass sample types was observed for the time data collected within this study, yet analysis of relevant data points within each individual sample type still produced appropriate trends. This is shown in Fig. 8, where the data collected for each biomass type is displayed along with the experiments in each environment. By approximating an oxy-combustion concentration based off this data, it can be estimated that oxygen levels ranging from 22 to 29% would be needed

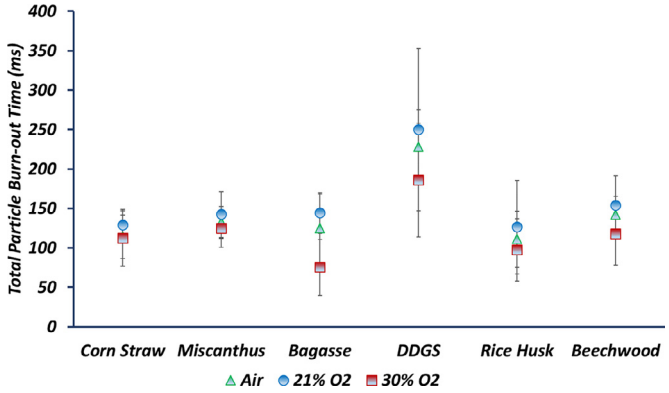


**Fig. 7.** Average measured total particle burnout times for all biomass fuels of this study burning with preheated input gases in a DTF, operated at $T_{wall}$ = 1400 K.

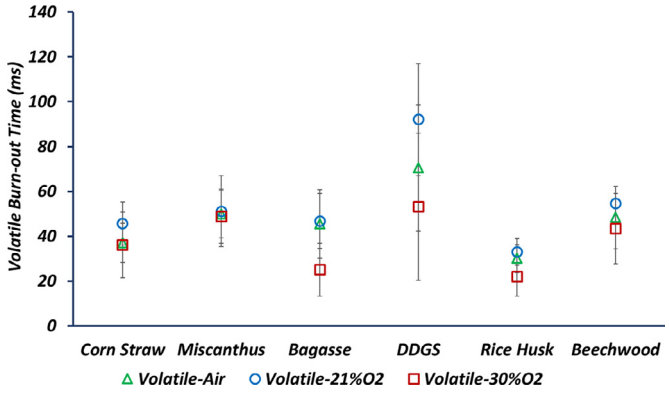


**Fig. 8.** Average measured volatile matter burn-out times for all biomass fuels of this study burning with preheated input gases in a DTF, operated at $T_{wall}$ = 1400 K.

to produce similar $t_v$ values to those in standard air. This wider range can be attributed to the variation between each biomass type.

### 3.4.2. Char burnout times

Similar to volatile matter burnout time, the char burnout time, $t_c$, refers to the duration of the char phase in the combustion process for a particle. Since the char phase is categorized by prolonged burning with lower temperatures, this data is typically longer than the time taken for the volatile phase, but is still important in fully capturing the nature of particle combustion and analyzing how varying oxygen environments alters this behavior. Values of $t_c$ were measured to be within the ranges of (80–125) ms, (50–100) ms, and (80–120) ms for 21%$O_2$ oxy-combustion, 30%$O_2$ oxy-combustion, and standard air combustion, respectively. The results for each individual biomass type that make up these ranges are displayed in Fig. 9. Employing the same method utilized for the prior properties discussed within this study, oxy-combustion oxygen levels ranging from 21 to 29% would be needed to create adequate $t_c$ values that mimic those of standard air combustion. The same variation seen within the $t_v$ study was displayed for the $t_c$ values collected here, creating a similarly wide range.

To investigate theoretically how varying the oxygen concentration in carbon dioxide diluent gas affects the char particle temperature and burnout time trends, numerical simulations were performed using a simplified char combustion model [47]. This task was undertaken to examine the influences of the involved physical parameters (oxygen partial pressure, binary molecular diffusivity, thermal conductivity, surface emissivity, etc.) the particle temperature and burnout times, as well as the possible influence of kinetic parameters (activation energy, etc.) on the

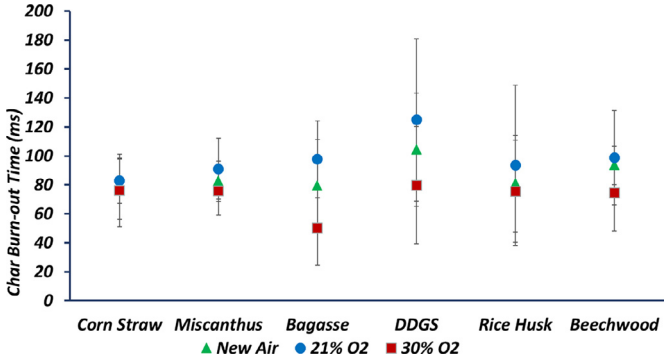


**Fig. 9.** Average measured char burn-out times for all biomass fuels of this study burning with preheated input gases in a DTF, operated at $T_{wall}$ = 1400 K.

particle temperature. The model is useful for examining trends in these parameters. Results are shown in the Appendix. A parametric study is also included therein. The simplified model for biomass char combustion in $O_2/CO_2$ environments, which have different molecular diffusivities, approximated reasonably well the measured beechwood char temperatures within ±50 K. It also approximated well the increasing temperature trend with increasing $O_2$ partial pressure. The char burnout times and their decreasing trends with increasing $O_2$ partial pressure, were also approximated reasonably well by the model, as the predictions fell within the parameter uncertainty bars.

### 3.5. Ignition delay times

Single torrefied biomass particles, in the 212–300 μm nominal size range, burning in air and oxy-combustion conditions ignited homogeneously forming envelope flames. This is in agreement with prior observations on biomass samples both raw and torrefied that were also burned in this experimental apparatus [33], where similar homogeneous ignition behavior was observed, and elsewhere in experiments involving raw pine sawdust particles [55]. Such behavior is expected, as the average char particle diameter, $X$, is larger than the critical particle diameter $X_c$, in air and in the $O_2/CO_2$ environments of this study, $X_c$, as defined by Howard and Essenhigh [48]. In this case, the volatile matter flame lifts away from the particle surface and distinct volatile and char burning modes occur [37,49]. Herein, the ignition delay was defined based on still frames of back-lit cinematography. It has been taken as the elapsed time from the moment when a particle was recorded to exit the water-cooled DTF injector to the moment when particle-related luminosity became visually apparent, see for example Fig. 2. Particle ignition delays derived with this method are displayed in Fig. 10 for all the torrefied biomass fuels of this study. Therein it is shown that the ignition delay of torrefied biomass particles increases with decreasing oxygen concentration, which is in agreement with the results of Simões et al. [37] and Austin et al. [50] for ignition delays of biomass particles burning in $O_2/N_2$ mixtures. Moreover, the ignition delay of these particles increased when the background $N_2$ gas was replaced with $CO_2$, as also observed by Lei et al. in combustion of raw pine sawdust particles [55]. There have been some additional reports [37,51,52] on the ignition behavior of raw biomass, however, studies on the ignition of torrefied biomass fuels are scarce.

The observed timing of homogeneous (gas-phase) ignition of devolatilizing fuel particles depends on the transport properties of the surrounding gas and on the reactivity of the local fuel-oxidizer mixture [51,53]. Specifically, auto-ignition of the local mixture depends on the local oxygen concentration, the local gas temperature and the local concentration and type of volatile species. Ignition

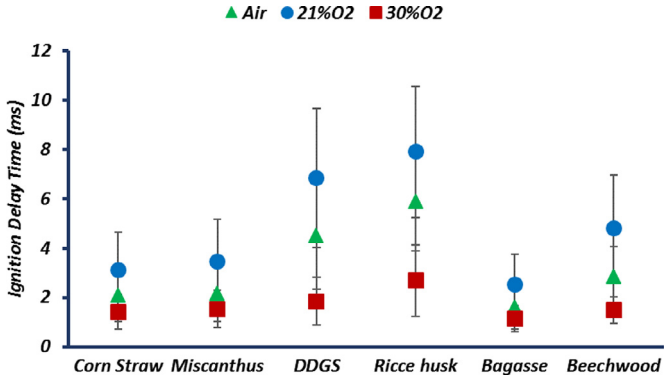


**Fig. 10.** Torrefied biomass particle ignition delay times, in preheated input gasses in a DTF, for various particle size cuts in the DTF operated at $T_{wall}$ = 1400 K ($T_{gas}$=~1350 K).

delay time decreases as the mixture reactivity and heat release increase. To the contrary, ignition delay time increases as the product of the molar heat capacity and density of the gas ($\rho C_p$) increases [53]. As a result, volatiles released in higher oxygen concentration gases ignite faster [37] and, also, volatiles released in $O_2/N_2$ mixtures ignite faster than those released in $O_2/CO_2$ mixtures of the same $O_2$ concentration. These trends are in line with the experimental results plotted in Fig. 10. For more information on the ignition delay and relevant equations, the interested reader is referred to Refs. [37,39,54], which pertain to coal particle ignition.

### 3.6. Oxygen concentration approximation

If a specific oxygen level were to be reached that would ultimately produce the same behavior in oxy-combustion to that of air combustion, all the properties previously presented must be taken in to account. However, within the ranges shown for each property, there is a large degree of variation between any specific biomass type. For this reason, desired oxygen levels that are based on a specific biomass sample alone were sought, as combining various types will produce general, irrelevant conclusions that do not adequately capture the nature of several samples. Oxygen concentrations for all six biomass samples were estimated in place of a sole threshold to mimic air combustion behavior. In order to simply take the average oxygen levels generated by all the properties for each biomass, it must first be concluded that any variation between these levels is simply due to experimental imperfection, i.e., the true average oxygen level for any given biomass type is the same for all properties analyzed and any differences observed within the experimental data are simply due to variance, caused by particle to particle variability. Performing an analysis of variance (ANOVA) test concluded that, with 95% confidence, the desired oxygen concentration for any individual biomass type is the same for each property present in this study. This allows for an average oxygen level to be taken for each sample. This level would serve as a benchmark to be retested at and have the resulting combustion behavior data comparable to that of air combustion. The generated oxygen levels for each biomass type analyzed are shown in Table 2.

To confirm these generated oxygen levels, experimental oxy-combustion trials were again conducted for each biomass at their specific estimated oxygen concentration. The data collected from these experiments was then compared to the air combustion data previously captured. This comparison can be seen in Fig. 11 for each of the five properties discussed within the scope of this paper. There was good agreement between the new oxy-combustion data (labeled "*Oxy*" in Fig. 11) and the respective air combustion data (labeled "*Air*" in Fig. 11), affirming that the estimated oxygen concentrations are satisfactory.

**Table 2**
Average estimated oxygen concentrations in carbon dioxide which would mimic the combustion behavior of standard air combustion for all biomass fuels of this study.

| Biomass type | Oxygen concentration |
|---|---|
| Corn Straw | 29% |
| Miscanthus | 27% |
| Bagasse | 24% |
| DDGS | 23% |
| Rice Husk | 25% |
| Beechwood | 25% |

The original hypothesis presented within this study initially predicted that the necessary oxygen concentrations would be proportional to known chemical and physical properties of the fuel. The parameters taken into account to decipher this correlation within the scope of this work were the fuel's oxygen content (O wt%), hydrogen content (H wt%), carbon content (C wt%), volatile matter (VM wt%), heating value (HV in MJ/kg), and initial aspect ratio (AR). Using these properties, the following empirical relationship was constructed in order to be able to predict the necessary oxygen concentrations ($[O_2']$ required for oxy-combustion to produce similar combustion behavior to air combustion:

$$[O_2'] = 8.177 * \left(\frac{H\%}{O\%}\right)\left(\frac{H\%}{C\%}\right)\left(\frac{VM\%}{HV \times AR}\right) + 0.1466 \quad (1)$$

Where the concentrations and volatile matter parameters are inputted as mass percentages and the heating value as MJ/kg.

Out of the six biomass samples analyzed, DDGS was left out of this relationship due to its tendency to burn in aggregates of multiple particles rather than as single particles. This skewed the correlation and consequently the sample was omitted. To test the applicability of this relationship to other materials, coal data from previous works in this laboratory [49], as well as bituminous coal and pine sawdust samples from another study [55] were included to see if predicted concentrations agreed with the collected experimental data in those studies. In addition, published data on several other bituminous and sub-bituminous coal samples from various studies were also included to further assess the derived correlation [56–61].

The correspondence between the predicted and experimental oxygen concentrations can be seen in Fig. 12. Evident from the plot, there is a satisfactory correlation between the values predicted from the derived formula and the experimental findings. Riaza et al. [31] did not give recommendations for appropriate oxygen concentrations in their study of oxy-combustion of coal and biomass; they only mentioned that "the 30%$O_2$ atmosphere was enough to have less burnout time than in air atmosphere for all the samples". Nevertheless, based on the data presented in their publication and using Eq. (1) the oxygen mole fraction requirement for their coal is calculated to be 27%, whereas that for their white wood is calculated to be 23%. Then, given their experimental burnout time differences between combustion in air, in 21%$O_2/CO_2$ and in 30%$O_2/CO_2$ as they appear in their Fig. 4, these predicted values are deemed to be satisfactory.

The parameters in this equation are based on their perceived influences on combustion. Various arrangements of these parameters were attempted, and the one that gave the best result was selected. The placement of the oxygen content in the denominator can be readily explained by the fact that the higher the oxygen content in the fuel the lower the need for atmospheric oxygen to complete the combustion. The placement of the other parameters is perhaps less clear and needs some explanation for their roles.

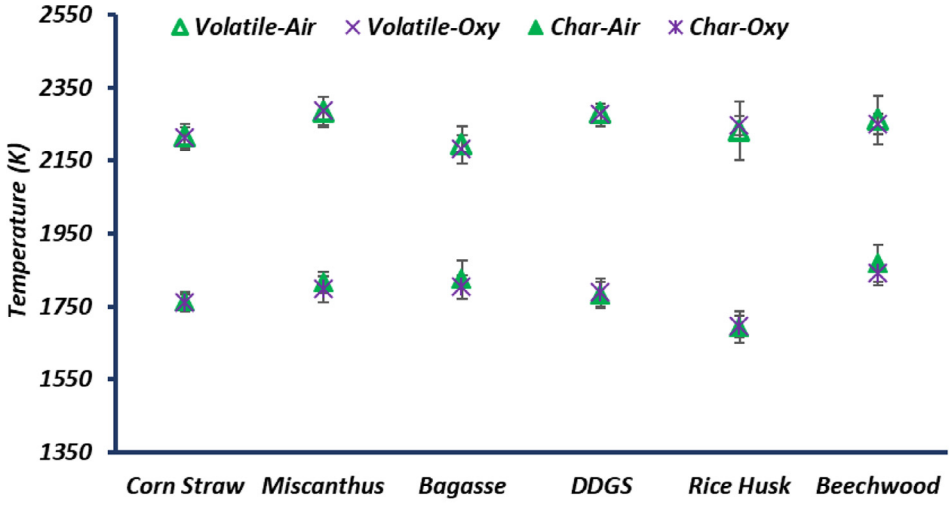


(a)

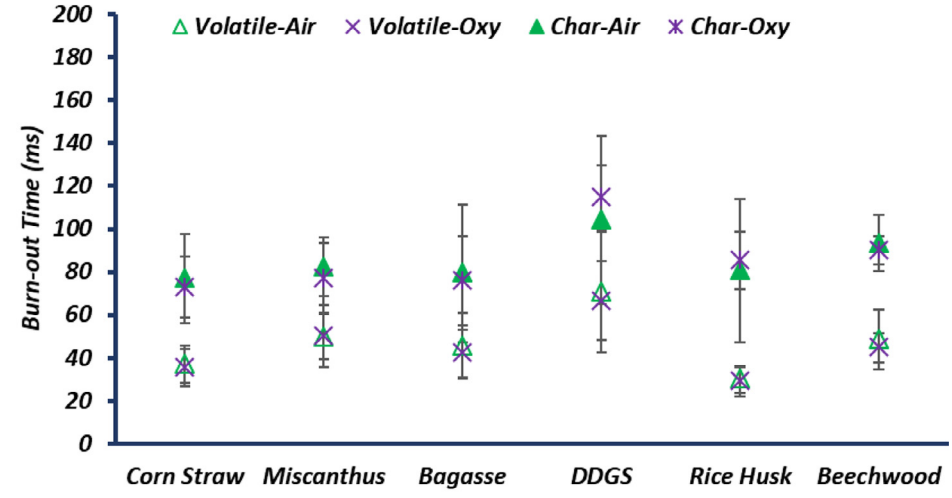


(b)

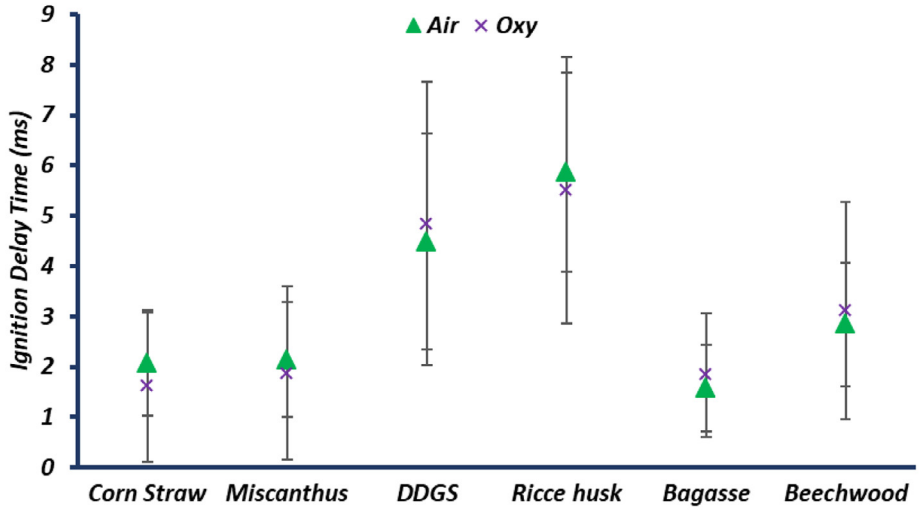


(c)

**Fig. 11.** Average measured [(a) Volatile Matter Temperatures (K) and Char Temperatures (K) (b) Volatile Matter Burnout Times (ms) and Char Burnout Times (ms) (c) Ignition Delay Times (ms)] for all biomass fuels of this study, burning in the DTF operated at $T_{wall}$ = 1400 K in air and in selected oxygen level. "*Oxy*" in these plots signifies oxy-combustion of the biomass particles at the average interpolated oxygen mole fractions displayed in Table 2.

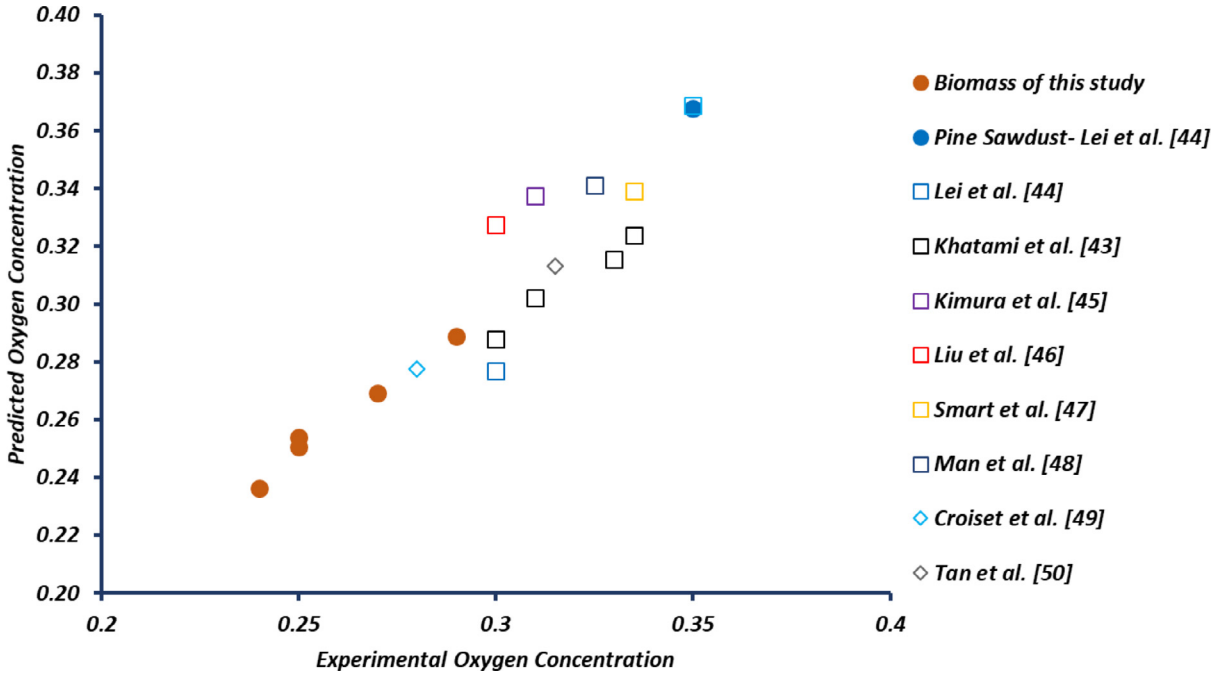


**Fig. 12.** Oxygen requirement for oxy-combustion to mimic combustion of single particles of biomass and coal fuels in air. Experimentally determined values are compared to predicted values using Eq. (1). Points indicated by solid brown circles refer to the torrefied biomass fuels of this study. Points indicated by hollow squares refer to bituminous coal. Points indicated by hollow diamonds refer to a sub-bituminous coal.

The placement of the heating value of the fuel in the denominator signifies that energy released from higher heating value fuels may compensate for small deficiencies in environmental oxygen. The placement of the particle aspect ratio in the denominator may be justified by the fact that higher initial aspect ratios lead to higher surface areas and more surface edges, which can be “hot spots” for ignition sites [62]. Such surface morphologies can allow particles to readily encounter oxygen and, hence, ignite promptly and burn more effectively even at lower oxygen concentrations. The volatile matter content was placed in the numerator based on the following reasoning. The released volatiles diffuse in air and burn homogeneously. As a result, the oxygen in the vicinity of the particle gets temporarily depleted. The higher the amount of volatile matter the greater the degree of oxygen depletion. The ensuing heterogeneous combustion of char is then temporarily compromised by the lack of oxygen. To compensate for this deficiency, an enhancement of the oxygen concentration in the gas can enable the char combustion to proceed faster. Moreover, as hydrogen readily evolves through hydrogen abstraction, according to the HACA mechanism [63], a fuel with higher hydrogen to carbon ratio is likely to demand more amospheric oxygen in the formation of radical intermediates and water. In addition, experiments in internal combustion engines under fuel-rich conditions have indicated a higher tendency of oxygen to bond with hydrogen in the hydrocarbon fuel and form water rather than to bond with carbon and form carbon oxides. Under such conditions, where oxygen is scarce, hydrogen preferentially reacts with oxygen and little unreacted hydrogen remains in the form of $H_2$; to the contrary, more partially reacted carbon remains in the form of CO [64]. Consequentially, the oxygen demand would be proportional to the H/C ratio and, also, to the H/O ratio of the fuel. It should be of note that the main source of uncertainty within this correlation rests with the initial aspect ratios of the fuels in question. Volatile matter and heating value data was obtained from an outside lab and their accuracy can be considered reasonably reliable. The initial aspect ratios, on the other hand, have wide ranges and vary on a particle to particle basis. Altering the initial aspect ratio causes the predicted oxygen concentrations to differ significantly. Thus, aspect ratios were carefully chosen from microscopic observation of biomass particles to obtain accurate representations. In the case of fuels (coals) adopted from the literature, for inclusion in Fig. 12, if aspect ratios were not reported then aspect ratios were chosen within the reasonable ranges for similar coals typically reported in the literature.

Investigations on burning single particles are valuable in discerning fundamental physical and chemical parameters governing the processes of ignition and combustion. At the absence of such studies, assessment of the impact of key parameters on these processes would not have been possible. Hence, this study follows the combustion histories of single particles. From a practical view point the acquired knowledge may be directly applicable to dilute suspensions of particles that exist away from a burner ($l/a$ >25, where $a$ is the particle radius and $l$ is the inter-particle spacing [65]). Such measurements can probe a limiting case that is well-enough defined to be useful for testing models for particle devolatilization and combustion processes [66]. However, in dense suspensions of particles, which prevail in the core of sprays, particles do not burn isolated and interactions among neighboring particles may impact on their drag coefficients, modify their ignition behaviors, affect their ignition delays, induce competition for heat and oxygen, and alter the bulk gas composition around the particles [65]. Hence, we recommend that the simple method of this investigation, based on the ignition and combustion of isolated particles, be used only for preliminary predictions. Confirmation should be provided by additional large-scale tests at the presence of streams of particles, where more definite assessments can be made, such as by measurement of the amount of unburned carbon in the ash.

Finally, it should be kept in mind that oxy-combustion of biomass, combined with carbon dioxide capture and utilization or sequestration can be beneficial to the atmospheric environment; however, it can also be costly. For instance, the energy consumption costs associated with the cryogenic generation of oxygen at

the air separation unit are significant. They have been estimated to reaching 685 kJ/kg of $O_2$ produced [67]. For example, in the case of beechwood, this energy cost yields an energy penalty of roughly 5.2% assuming stochiometric conditions for the $m_{fuel}/m_{oxygen}$ ratio and taking into account the heating value present within the fuel. This calculation also assumes that the full energy capable of being extracted from the fuel is harnessed and the plant efficiency in question is 100%, which is of course unrealistic. A lower plant efficiency, say 33%, will cause this penalty to increase by a factor of three. There are also many other costs, such as those associated with the purification and compression of the exhaust stream and with procurement and torrefaction of the biomass.

## 4. Conclusions

This research addressed the oxy-combustion behavior of single torrefied biomass particles. Finding the oxygen concentration threshold within oxy-combustion that allows for the behavior of biomass fuels to mimic that in air combustion is pivotal in optimizing the oxy-combustion process and allowing for the most ideal integration of the process over standard air burning. This threshold is desirable in practice, as surpassing the estimated oxygen concentration yields higher energy costs with unnecessary oxygen being inputted into the furnace, whereas going under the estimated oxygen concentration yields lower fuel utilization efficiency and unburned carbon in the flue gases. This study tested six types of pulverized torrefied biomass fuels (212–300 μm) in $O_2/CO_2$ atmospheres as well as in standard air, within a DTF, and key combustion temperatures and times were monitored as the basis for analysis. Interpolation methods were utilized once data for 21% oxygen concentrations and 30% oxygen concentrations in $CO_2$ was collected to estimate the oxygen concentration needed to yield similar property magnitudes to those found from air combustion. It was found, through the methodology of this work, that the oxygen levels needed for oxy-combustion to produce similar combustion parameter values to those encountered in standard air combustion vary between each type of biomass analyzed, ranging from 23 to 29%. Hence, the selection of the biomass fuel in practice will be the driving factor for the minimum oxygen requirements. The oxygen concentrations discussed previously allow for the correct proportions of $O_2/CO_2$ to adequately mimic the volume ratio of standard air for the biomass fuels within the scope of this study, evident by the analysis of combustion volatile temperature, char temperature, volatile matter burnout time, char burnout time, and total combustion burnout time. A correlation between various chemical and physical properties of each fuel was derived in order to conduct preliminary predictions of these concentrations.

## Declaration of interests

The authors declare that they have no known competing financial interests or personal relationships that could have appeared to influence the work reported in this paper.

## Acknowledgments

This work was supported by the US National Science Foundation Grant # 1810961. The authors would like to thank Dr. Xiaohan Ren at Harbin Institute of Technology for his assistance in conducting the proximate and ultimate analysis of the fuels.

## Appendix: Calculated Char Temperature and Char Burnout Time Based on Simplified Modeling

This section explores the char particle *T-t* trends and magnitudes and compares the experimental data of this study (including the data obtained in Section 3) with results from Field's particle combustion model [47]. To obtain meaningful results, several properties of the chars from these particles needed to be measured, hence, separate experiments were conducted in order to collect sufficient quantities for characterization of chars. Beechwood was chosen as the biomass fuel for these additional experiments, since several of its key physical and chemical parameters were already available in the literature. This specific biomass fuel also yielded repeatable pyrometer readings during experimentation. Samples of raw beechwood were grinded, sieved, and torrefied in preparation for combustion in a different DTF under the same high heating rate and temperature conditions. The generated chars were collected at the bottom outlet of the furnace. Scanning electron microscope photographs were taken of both the chars and the resulting ashes, shown in Fig. 4. When beechwood biomass is devolatilized under the high heating rates ($10^4$ K/s) of the DTF and of utility suspension boilers, undergoes fusion and spherodization, see also [38].

Beechwood char collected in these experiments was sent to an external laboratory (*Micromeritics Instrument Corporation*) to measure its skeletal and bulk densities, using helium gas pycnometery and mercury porosimetry, respectively. These densities are reported within Table A1. It can be concluded that Beechwood char is highly porous, as also attested by the SEM photographs shown in Fig. 4 of the main text.

**Table A1**
Reported densities for the beechwood char samples.

| | |
|---|---|
| Skeletal density (g/cm$^3$) | 1.7543 |
| Bulk density (g/cm$^3$) | 0.1597 |

**Table A2**
Biomass particle properties and furnace operating parameters input to the base model.

| | | |
|---|---|---|
| $p_g$ | Partial pressure of oxygen, atm | 0.20–0.30 |
| $A$ | Pre-exponential factor, g/cm$^2$ s atm | 18 [74] |
| $E$ | Activation energy, cal/mole | 19,000 [74] |
| $R$ | Gas constant, cal/mole K | 1.986 |
| $T_g$ | Gas temperature, K | 1350 [23] |
| $T_s$ | Char surface temperature, K | From Fig. 6 |
| $T_m$ | Mean Temperature, $(T_g+T_s)/2$, K | Varies |
| $\Delta H$ | Heat release at surface per unit mass of carbon burnt, cal/g | 2340 [72] |
| $D$ | Diffusion coefficient of oxygen in the gas, cm$^2$/s | Varies with $T_s$ [75] |
| $k_s$ | Surface reaction rate coefficient, g/cm$^2$ s atm | Eq. (8) |
| $k_{diff}$ | Diffusion reaction rate coefficient, g/cm$^2$ s atm | Varies |
| $x$ | Char particle diameter, cm | 0.0245 ± 0.0035 cm |
| $\sigma$ | Stefan-Boltzmann constant, cal/cm$^2$ s K$^4$ | $1.36 \times 10^{-12}$ |
| $\epsilon$ | Emissivity | 0.9 [38] |
| $\lambda_0$ | Thermal conductivity at gas temperature, cal/cm s K | 0.0002 for air, 0.000212 for 20% $O_2$/80% $CO_2$, 0.000213 for 30% $O_2$/70% $CO_2$ |
| Q | Heat release at surface per unit mass of carbon burned, cal/g | 2340 [72] |

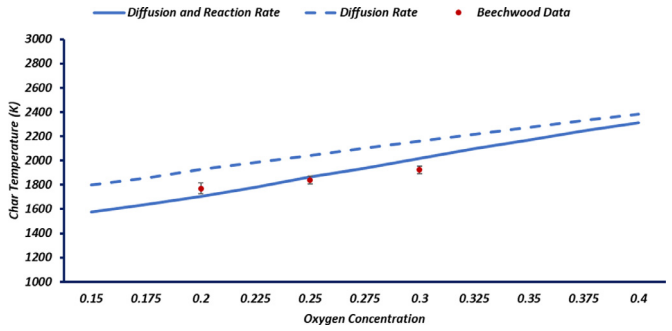


**Fig. A1.** Predicted beechwood char temperatures and the relevant experimental data versus oxygen concentration level.

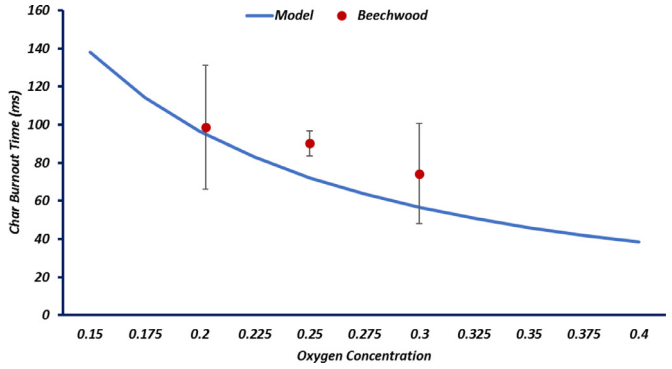


**Fig. A2.** Predicted beechwood char burnout times (for Regime III) and experimentally-obtained burnout times versus oxygen concentration level.

The char combustion model utilized within this study is based off the model presented by Field [47] in which the particle in question is considered to be in thermal equilibrium, with both the rate of heat generation and rate of heat loss being equal [68,69]. This gives:

$$H_g = H_c + H_r \tag{2}$$

Where $H_g$ refers to the rate of heat generation for the particle, $H_c$ is conduction heat loss, and $H_r$ is radiation heat loss. Each of these terms is a function of particle temperature, so by expressing them as such, it is possible to estimate the char temperature that would be necessary for thermal equilibrium. The conduction heat loss can be expressed as:

$$H_c = 2\lambda_0 \left(\frac{T_s + T_g}{2T_g}\right)^{0.75} \times \frac{(T_s - T_g)}{x} \tag{3}$$

In Eq. (2), $\lambda_0$ refers to the thermal conductivity of the gas at the given gas temperature, $T_g$ is the gas temperature set at 1350 K for this study [23], and $x$ is the char particle diameter.

Similarly, the radiation heat loss is given by:

$$H_r = \epsilon\sigma\left(T_s^4 - T_w^4\right), \tag{4}$$

Where $T_w$ is the effective wall temperature of the surrounding surfaces, $\epsilon$ is the emissivity of the char particle, as a first approximation assumed to be 0.9 [38,70], and $\sigma$ is the Stefan-Boltzmann constant, in $\frac{\text{cal}}{\text{cm}^2.\text{s.K}}$.

The rate of heat generation can be expressed as:

$$H_g = qQ \tag{5}$$

Where $Q$ is the heat release at the char surface per unit mass of carbon burnt. This rate assumes that carbon is oxidized by oxygen and that predominant primary product of oxidation is CO at the elevated char particle temperatures of this study, see Ref. [71] and references therein. Thence, the value of $Q$ was taken as $2340\frac{\text{cal}}{\text{g}}$ [72], The parameter $q$ is the overall particle burning rate per unit external surface area. The $q$ term is a function of the partial pressure of oxygen, $p_g$, along with the reaction rate coefficients $k_{diff}$and $k_s$. This means that the burning rate $q$ will vary as the oxygen concentration is altered to form the model with variable oxygen levels as desired. Assuming that the apparent reaction of carbon order with oxygen is unity [73], the burning rate, $q$, for diffusion controlled (Regime III) reaction is given as:

$$q = \frac{p_g}{\left(\frac{1}{k_{diff}}\right)} \tag{6}$$

If the reaction is controlled by both diffusion and chemical reaction (Regime II) then the burning rate, $q$, is given as:

$$q = \frac{p_g}{\left(\frac{1}{k_{diff}} + \frac{1}{k_s}\right)} \tag{7}$$

The $k_s$ term refers to the surface chemical reaction rate and is given by an Arrhenius-type expression that depends on the rate constant of a chemical reaction on the absolute temperature, which in turn depends on the activation energy and a pre-exponential frequency factor [74]:

$$k_s = A\exp\left(-\frac{E}{RT_s}\right) \tag{8}$$

Where $A$ is the pre-exponential factor and $E$ is activation energy. The values of two parameters were taken from the literature [74] as 18 $\frac{g}{\text{cm}^2\text{s.atm}}$and 19,000 $\frac{\text{cal}}{\text{mole}}$.

The diffusional reaction rate coefficient, $k_{diff,}$ is given by:

$$k_{diff} = \frac{48\ D}{xRT_m} \tag{9}$$

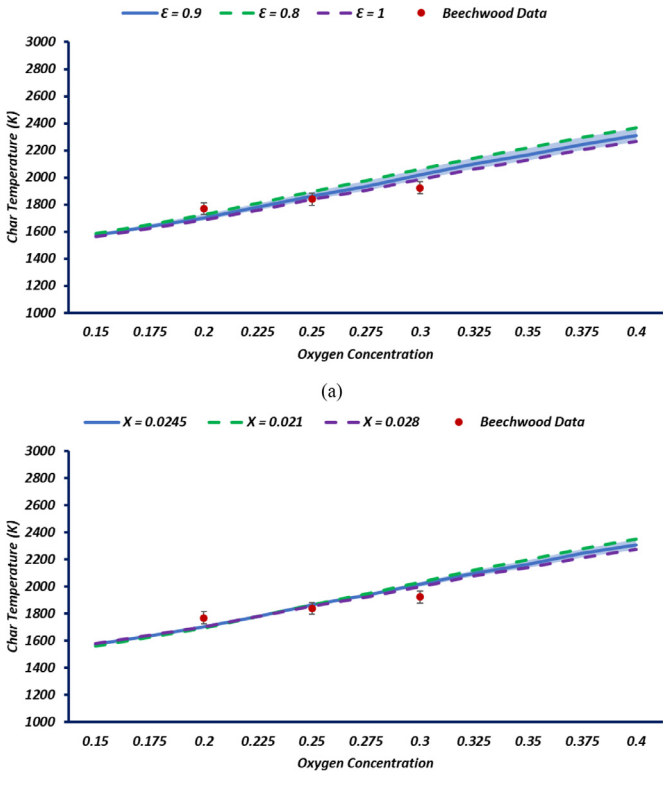


**Fig. A3.** The resulting char temperature model as the parameters of (a) emissivity, $\varepsilon$, (b) particle diameter, $x$, (c) activation energy, $E$, (d) pre-exponential factor $A$, are altered between a lower threshold, a selected baseline, and a higher threshold.

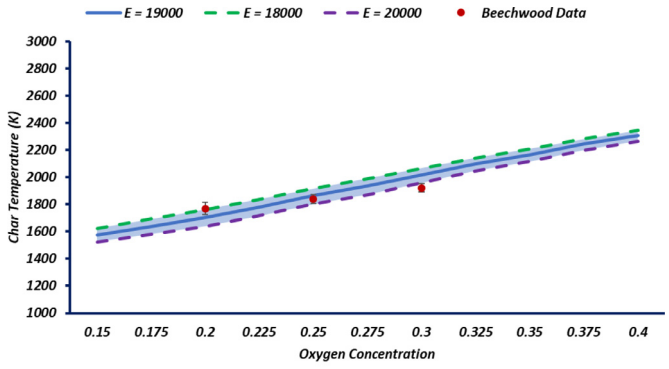


(c)

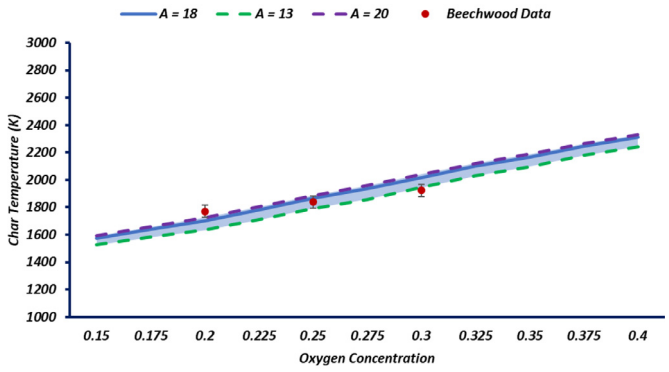


(d)

**Fig. A3.** Continued

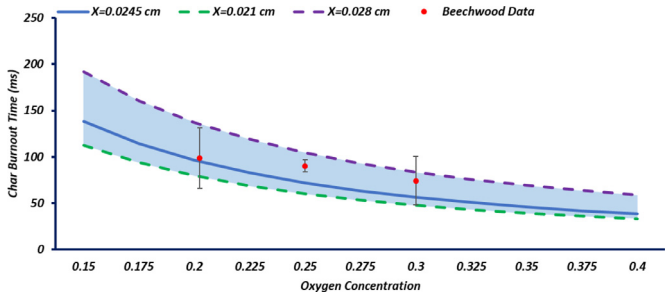


**Fig. A4.** The resulting char burnout time model as the particle diameter parameter, *x*, is altered between a lower threshold, its baseline ($X = 0.0245$ cm), and a higher threshold.

Where $R$ is the universal gas constant, in the units of $\frac{cal}{\text{mole.K}}$, and $D$ is diffusion coefficient of oxygen in the $CO_2$ gas, in $\frac{\text{cm}^2}{\text{s}}$, [75] and can be determined using the equation:

$$D = D_0\left(\frac{T_m}{T_0}\right)^{1.75} \tag{10}$$

Where $D_0$ and $T_0$ are a reference diffusivity coefficient and reference temperature, with values of 0.16 and 293 K respectively.

In this analysis the effects of gasification reactions between carbon and carbon dioxide were neglected, as explained in the main text.

A summary of the values used in the model are given in Table A2.

The predicted beechwood char temperatures derived from the above model equations, as a function of varying oxygen concentrations, and the experimental data collected from beechwood during this study are displayed together in Fig. A1. The comparison of the experimental results with the results of this simplified model suggests that the diffusion and reaction rate is more descriptive of the combustion of these chars, i.e., upper end of Regime II.

Given that the biomass char particles appear to be highly cenospheric with "pop-corn" like structure with voids that are mainly spherical bubbles, rather than cylinders, and with large blowholes that punctuate their surfaces; such structures would favor some penetration to their interiors, particularly after the walls between the bubbles get penetrated during the early stages of combustion [76]. In this case, combustion could have occurred at the high end of the high Regime II, with chemical reactions playing only a limited role.

The burnout time can be obtained from the following equation, which in Field's model is calculated for diffusion limited combustion (Regime III) [47]:

$$t_b = \frac{RT_m}{56D\ln\left(1 + {}^3\!/_4 Y_{O_2}\right)} \tag{10}$$

Where $R$ term is the universal gas constant and $T_m$ is the mean film temperature, given by the Fields model previously discussed, while $Y_{O_2}$ is the concentration of oxygen in the environment. Using Eq. (10), the predicted beechwood char burnout times were calculated as a function of varying oxygen concentrations and superimposed with the experimental data gathered within this study, shown in Fig. A2. As expected, based on the discussion above, Eq. (10) somewhat under-predicts the experimental burnout-times, as it is derived for diffusion limited combustion (Regime III).

Due to the uncertainty present for the values of several parameters, a sensitivity analysis was conducted to assess how the models react as these values are altered within reasonable ranges. In this analysis, the diffusion and reaction model (Regime III) was used. The parameters within question are the particle diameter, $X$, emissivity, $\varepsilon$, the pre-exponential factor, $A$, and the activation energy, $E_a$. Both minimum and maximum thresholds were considered for each value while the remaining three parameters were left constant. The resulting trends for the temperature prediction were analyzed.

The resulting model trends on the predicted char particle temperature as the emissivity parameter is changed can be seen in Fig. A3(a). A lower emissivity caused the char temperature to increase slightly, whereas a higher emissivity causes the temperature to decrease slightly. However, it is not conclusive which emissivity value works best. Next, the impact of altering the char particle diameter, $x$, in the range of $0.0245 \pm 0.035$ cm on both the temperature and burnout time can be seen in Figs. A3(b) and A4, respectfully. This trend shows that, as the particle diameter decreases in the examined range, the resulting char temperature increases slightly. The burnout time displays a much larger dependence on particle diameter. The lower and higher diameter thresholds create a large gap between each respective time model iteration, with a lower diameter yielding a shorter char burnout time and a higher diameter yielding a longer char burnout time.

The results of perturbing the activation energy can be seen in Fig. A3(c). The char temperature increased when the activation energy was lowered, and the char temperature decreased when the activation energy was amplified. The trends observed from altering the pre-exponential factor are displayed in Fig. A3(d). When this factor was decreased the resulting char temperature also was lowered and vice versa for when the factor was increased.

This simple theoretical study affirms the trends observed during the experimentation phases for both char temperature and char burnout time of Beechwood char particles. Both predictions and experiments showed a gradual increase in char temperature as the oxygen concentration in carbon dioxide diluent gas increased, with this growth being less prominent at lower oxygen levels. This trend is less apparent based on solely the experimental data, as

the range within the experimental scope was limited to 21–30%, but the model data depicts the pattern more clearly. In terms of char burnout times, the model predicts a decline in this parameter as the oxygen levels increased, but there are diminishing returns to this process, as continuing to further increase oxygen concentrations eventually will bring estimates to a plateau where a minimum burnout time is reached. Again, this trend is hard to see from the experimental data alone due to the narrower range analyzed.

## References


[1] U.S. Energy Information Administration, EIA Total Energy Data.
[2] A. Akella, R. Saini, M.P. Sharma, Social, economical and environmental impacts of renewable energy systems, Renew. Energy 34 (2009) 390–396.
[3] E. Rokni, A. Panahi, X. Ren, Y.A. Levendis, Curtailing the generation of sulfur dioxide and nitrogen oxide emissions by blending and oxy-combustion of coals, Fuel 181 (2016) 772–784.
[4] S.K. Sirumalla, A. Panahi, A. Purohit, A. Baugher, Y.A. Levendis, R.H. West, Nitrogen Oxide Evolution in Oxy-Coal Combustion, US Eastern States Section of the Combustion Institute, 2018.
[5] A. Panahi, S.K. Sirumalla, R.H. West, Y.A. Levendis, Temperature and oxygen partial pressure dependencies of the coal-bound nitrogen to $NO_x$ conversion in $O_2/CO_2$ environments, Combust. Flame 206 (2019) 98–111.
[6] E. Biagini, F. Lippi, L. Petarca, L. Tognotti, Devolatilization rate of biomasses and coal–biomass blends: an experimental investigation, Fuel 81 (2002) 1041–1050.
[7] S.G. Sahu, N. Chakraborty, P. Sarkar, Coal–biomass co-combustion: an overview, Renew. Sustain. Energy Rev. 39 (2014) 575–586.
[8] D.R. Nhuchhen, P. Basu, B. Acharya, A comprehensive review on biomass torrefaction, Int. J. Renew. Energy Biofuels 2014 (2014) 1–56.
[9] A. Demirbas, Potential applications of renewable energy sources, biomass combustion problems in boiler power systems and combustion related environmental issues, Progr. Energy Combust. Sci. 31 (2005) 171–192.
[10] P. McKendry, Energy production from biomass (part 1): overview of biomass, Bioresour. Technol. 83 (2002) 37–46.
[11] Q.-.V. Bach, Ø. Skreiberg, Upgrading biomass fuels via wet torrefaction: a review and comparison with dry torrefaction, Renew. Sustain. Energy Rev. 54 (2016) 665–677.
[12] W.-.H. Chen, J. Peng, X.T. Bi, A state-of-the-art review of biomass torrefaction, densification and applications, Renew. Sustain. Energy Rev. 44 (2015) 847–866.
[13] J. Chew, V. Doshi, Recent advances in biomass pretreatment–Torrefaction fundamentals and technology, Renew. Sustain. Energy Rev. 15 (2011) 4212–4222.
[14] S. Sadaka, S. Negi, Improvements of biomass physical and thermochemical characteristics via torrefaction process, Environ. Prog. Sustain. Energy 28 (2009) 427–434.
[15] T. Bridgeman, J. Jones, I. Shield, P. Williams, Torrefaction of reed canary grass, wheat straw and willow to enhance solid fuel qualities and combustion properties, Fuel 87 (2008) 844–856.
[16] D. Magalhães, A. Panahi, F. Kazanç, Y.A.J.F. Levendis, Comparison of single particle combustion behaviours of raw and torrefied biomass with Turkish lignites, Fuel 241 (2019) 1085–1094.
[17] E. Rokni, X. Ren, A. Panahi, Y.A. Levendis, Emissions of $SO_2$, $NO_x$, $CO_2$, and HCl from co-firing of coals with raw and torrefied biomass fuels, Fuel 211 (2018) 363–374.
[18] X. Ren, X. Meng, A. Panahi, E. Rokni, R. Sun, Y.A. Levendis, HCl release from combustion of corn straw in a fixed bed, J. Energy Resour. Technol. 140 (5) (2017) 051801.
[19] D. Agar, M. Wihersaari, Bio-coal, torrefied lignocellulosic resources – key properties for its use in co-firing with fossil coal – their status, Biomass Bioenergy 44 (2012) 107–111.
[20] R.B. Bates, A.F. Ghoniem, Biomass torrefaction: modeling of reaction thermochemistry, Bioresour. Technol. 134 (2013) 331–340.
[21] R.H. Ibrahim, L.I. Darvell, J.M. Jones, A. Williams, Physicochemical characterisation of torrefied biomass, J. Anal. Appl. Pyrolysis 103 (2013) 21–30.
[22] M. Van der Stelt, H. Gerhauser, J. Kiel, K. Ptasinski, Biomass upgrading by torrefaction for the production of biofuels: a review, Biomass Bioenergy 35 (2011) 3748–3762.
[23] A. Panahi, Y.A. Levendis, N. Vorobiev, M. Schiemann, V. Scherer, Combustion behavior of herbaceous and woody biomass, 41st International Technical Conference on Clean Coal and Fuel Systems, Clearwater, Florida, USA (2016), pp. 62–72.
[24] J. Riaza, M. Gil, L. Álvarez, C. Pevida, J. Pis, F. Rubiera, Oxy-fuel combustion of coal and biomass blends, Energy 41 (2012) 429–435.
[25] B.J. Buhre, L.K. Elliott, C. Sheng, R.P. Gupta, T.F. Wall, Oxy-fuel combustion technology for coal-fired power generation, Prog. Energy Combust. Sci. 31 (2005) 283–307.
[26] L. Chen, S.Z. Yong, A.F. Ghoniem, Oxy-fuel combustion of pulverized coal: characterization, fundamentals, stabilization and CFD modeling, Prog. Energy Combust. Sci. 38 (2012) 156–214.
[27] B. Arias, C. Pevida, F. Rubiera, J. Pis, Effect of biomass blending on coal ignition and burnout during oxy-fuel combustion, Fuel 87 (2008) 2753–2759.
[28] A. Panahi, N. Toole, Y. Yang, M. Schiemann, Y.A. Levendis, Oxy-combustion behavior of torrefied biomass particles, 11th US National Combustion Meeting (2019).
[29] J. Riaza, R. Khatami, Y.A. Levendis, L. Álvarez, M.V. Gil, C. Pevida, F. Rubiera, J.J. Pis, Combustion of single biomass particles in air and in oxy-fuel conditions, Biomass Bioenergy 64 (2014) 162–174.
[30] F. Shan, Q. Lin, K. Zhou, Y. Wu, W. Fu, P. Zhang, L. Song, C. Shao, B. Yi, An experimental study of ignition and combustion of single biomass pellets in air and oxy-fuel, Fuel 188 (2017) 277–284.
[31] J. Riaza, M. Ajmi, J. Gibbins, H. Chalmers, Ignition and combustion of single particles of coal and biomass under $O_2/CO_2$ atmospheres, Energy Proc. 114 (2017) 6067–6073.
[32] L. Timothy, A.F. Sarofim, J.M. Beér, Characteristics of single particle coal combustion, Sympos. (Int.) Combust. 19 (1982) 1123–1130.
[33] A. Panahi, M. Tarakcioglu, M. Schiemann, M. Delichatsios, Y.A. Levendis, On the particle sizing of torrefied biomass for co-firing with pulverized coal, Combust. Flame 194 (2018) 72–84.
[34] A. Panahi, M. Tarakcioglu, Y.A. Levendis, Torrefied biomass size for combustion in existing boilers, 10th US National Combustion Meeting (2017).
[35] Y.A. Levendis, A. Panahi, E. Rokni, X. Ren, Emissions from cofiring coals, 40th International Technical Conference on Clean Coal and Fuel Systems, Clearwater, Florida, USA (2015), pp. 533–544.
[36] Y.A. Levendis, K.R. Estrada, H.C. Hottel, Development of multicolor pyrometers to monitor the transient response of burning carbonaceous particles, Rev. Sci. Instrum. 63 (1992) 3608–3622.
[37] G. Simões, D. Magalhães, M. Rabaçal, M. Costa, Effect of gas temperature and oxygen concentration on single particle ignition behavior of biomass fuels, Proc. Combust. Inst. 36 (2017) 2235–2242.
[38] A. Panahi, Y. Levendis, N. Vorobiev, M. Schiemann, Direct observations on the combustion characteristics of miscanthus and beechwood biomass including fusion and spherodization, Fuel Process. Technol. 166 (2017) 41–49.
[39] C.R. Shaddix, A. Molina, Particle imaging of ignition and devolatilization of pulverized coal during oxy-fuel combustion, Proc. Combust. Inst. 32 (2009) 2091–2098.
[40] A. Panahi, N. Vorobiev, M. Schiemann, M. Tarakcioglu, M. Delichatsios, Y.A. Levendis, Combustion details of raw and torrefied biomass fuel particles with individually-observed size, shape and mass, Combust. Flame 207 (2019) 327–341.
[41] T. Maffei, R. Khatami, S. Pierucci, T. Faravelli, E. Ranzi, Y.A. Levendis, Experimental and modeling study of single coal particle combustion in $O_2/N_2$ and oxy-fuel ($O_2/CO_2$) atmospheres, Combust. Flame 160 (2013) 2559–2572.
[42] R. Khatami, Y.A. Levendis, On the deduction of single coal particle combustion temperature from three-color optical pyrometry, Combust. Flame 158 (2011) 1822–1836.
[43] T. Panagiotou, Y. Levendis, M. Delichatsios, Measurements of particle flame temperatures using three-color optical pyrometry, Combust. Flame 104 (1996) 272–287.
[44] W. Reynolds, STANJAN, chemical equilibrium solver 1987, Department of Mechanical Engineering, Standford University, USA, 1981.
[45] P.A. Bejarano, Y.A. Levendis, Single-coal-particle combustion in $O_2/N_2$ and $O_2/CO_2$ environments, Combust. Flame 153 (2008) 270–287.
[46] I. Smith, The combustion rates of coal chars: a review, Symp. (Int.) Combust. 19 (1982) 1045–1065.
[47] M. Field, D. Gill, B. Morgan, P. Hawksley, Combustion of pulverized coal british coal utilization research association, Leatherland, UK, 1967.
[48] J. Howard, R. Essenhigh, Mechanism of solid-partical combustion with simultaneous gas-phase volatiles combustion, Symp. (Int.) Combust. 11 (1967) 399–408.
[49] R. Khatami, C. Stivers, K. Joshi, Y.A. Levendis, A.F. Sarofim, Combustion behavior of single particles from three different coal ranks and from sugar cane bagasse in $O_2/N_2$ and $O_2/CO_2$ atmospheres, Combust. Flame 159 (2012) 1253–1271.
[50] P. Austin, C. Kauffman, M. Sichel, Ignition and volatile combustion of cellulosic dust particles, Combust. Sci. Technol. 112 (1996) 187–198.
[51] A. Carvalho, M. Rabaçal, M. Costa, M. Alzueta, M. Abián, Effects of potassium and calcium on the early stages of combustion of single biomass particles, Fuel 209 (2017) 787–794.
[52] D. Magalhães, F. Kazanç, A. Ferreira, M. Rabaçal, M. Costa, Ignition behavior of Turkish biomass and lignite fuels at low and high heating rates, Fuel 207 (2017) 154–164.
[53] A. Molina, C.R. Shaddix, Ignition and devolatilization of pulverized bituminous coal particles during oxygen/carbon dioxide coal combustion, Proc. Combust. Inst. 31 (2007) 1905–1912.
[54] R. Khatami, C. Stivers, Y.A. Levendis, Ignition characteristics of single coal particles from three different ranks in $O_2/N_2$ and $O_2/CO_2$ atmospheres, Combust Flame 159 (2012) 3554–3568.
[55] K. Lei, B. Ye, J. Cao, R. Zhang, D. Liu, Combustion characteristics of single particles from bituminous coal and pine sawdust in $O_2/N_2$, $O_2/CO_2$, and $O_2/H_2O$ atmospheres, Energies 10 (2017) 1695.
[56] N. Kimura, K. Omata, T. Kiga, S. Takano, S. Shikisima, The characteristics of pulverized coal combustion in $O_2/CO_2$ mixtures for $CO_2$ recovery, Energy Convers. Manag. 36 (1995) 805–808.
[57] H. Liu, R. Zailani, B.M. Gibbs, Comparisons of pulverized coal combustion in air and in mixtures of $O_2/CO_2$, Fuel 84 (2005) 833–840.
[58] J. Smart, G. Lu, Y. Yan, G. Riley, Characterisation of an oxy-coal flame through digital imaging, Combust. Flame 157 (2010) 1132–1139.

[59] C.K. Man, J. Gibbins, Factors affecting coal particle ignition under oxyfuel combustion atmospheres, Fuel 90 (2011) 294–304.
[60] E. Croiset, K. Thambimuthu, A. Palmer, Coal combustion in $O_2/CO_2$ mixtures compared with air, Can. J. Chem. Eng. 78 (2000) 402–407.
[61] Y. Tan, E. Croiset, M.A. Douglas, K.V. Thambimuthu, Combustion characteristics of coal in a mixture of oxygen and recycled flue gas, Fuel 85 (2006) 507–512.
[62] Y.A. Levendis, R. Sahu, R.C. Flagan, G.R. Gavalas, Post-ignition transients in the combustion of single char particles, Fuel 68 (1989) 849–855.
[63] M. Frenklach, Reaction mechanism of soot formation in flames, PCCP 4 (2002) 2028–2037.
[64] O. Uyehara, A method to estimate H2 in engine exhaust and factors that affect NOx and particulate in diesel engine exhaust, Report No. 0148-7191, SAE Technical Paper, 1991.
[65] K. Annamalai, W. Ryan, Interactive processes in gasification and combustion—II. Isolated carbon, coal and porous char particles, Prog. Energy Combust. Sci. 19 (1993) 383–446.
[66] L. Timothy, D. Froelich, A. Sarofim, J. Beer, Soot formation and burnout during the combustion of dispersed pulverized coal particles, Symp. (Int.) Combust. (1988) 1141–1148.
[67] Y. Hu, X. Li, H. Li, J. Yan, Peak and off-peak operations of the air separation unit in oxy-coal combustion power generation systems, Appl. Energy 112 (2013) 747–754.
[68] D.A.b. Frank-Kameneckij, Diffusion and Heat Exchange in Chemical Kinetics, Princeton University Press, 1955.
[69] L.A. Vulis, Thermal Regimes of Combustion, McGraw-Hill, 1961.
[70] N. Vorobiev, A. Becker, H. Kruggel-Emden, A. Panahi, Y.A. Levendis, M. Schiemann, Particle shape and Stefan flow effects on the burning rate of torrefied biomass, Fuel 210 (2017) 107–120.
[71] Y.A. Levendis, A. Atal, J.B. Carlson, On the correlation of CO and PAH emissions from the combustion of pulverized coal and waste tires, Environ. Sci. Technol. 32 (1998) 3767–3777.
[72] N.V. Lavrov, The thermodynamics of gasification and gas-synthesis reactions, Pergamon Press, 1963.
[73] P.A. Bejarano, Y.A. Levendis, Combustion of coal chars in oxygen-enriched atmospheres, Combust. Sci. Technol. 179 (2007) 1569–1587.
[74] N. Vorobiev, M. Geier, M. Schiemann, V. Scherer, Experimentation for char combustion kinetics measurements: bias from char preparation, Fuel Process. Technol. 151 (2016) 155–165.
[75] W. Bartok, A.F. Sarofim, Fossil fuel combustion: a source book, Wiley Interscience, New York, 1991.
[76] M. Mulcahy, Kinetics of combustion of pulverized fuel: a review of theory and experiment, Pure Appl. Chem. 19 (1969) 81–108.